

REVIEW ARTICLE

Inorganic solid state chemically sensitive devices: electrochemical oxygen gas sensors

W C Maskell

Energy Technology Centre, Middlesex Polytechnic, Bounds Green Road, London N11 2NQ, UK

Abstract. The principles of operation of potentiometric, amperometric, coulometric and impedance-based oxygen gas sensors are reviewed. Factors influencing the speed of response are considered in detail and related to the information obtainable from impedance measurements. The response of a sensor to gaseous mixtures not in equilibrium is discussed, particularly in relation to measurements in gases generated by the combustion of fossil fuels.

1. Introduction

Several reviews of solid state gas sensors have been published during the last decade (Dietz *et al* 1977, Fouletier 1982/3, Williams and McGeehin 1984, Maskell and Steele 1986) and the reader is referred to these for background information including practical details and design of devices. The purpose of the present review is to concentrate on the scientific principles underlying the operation of the major device types rather than to describe the multitude of configurations available for technological applications. Where possible the discussion is generalised so as not to be specific to the sensing of a particular gas, whereas the examples refer to the sensing of oxygen. The attention devoted to the various device types reflects the relative volume of published literature relating to each. Many of the principles discussed for potentiometric sensors are applicable to devices operating in the alternative modes.

Solid state devices operating on electrochemical principles have gained popularity in some applications compared, for example, with aqueous electrochemical sensors for a number of reasons: the electrolyte in the former devices is non-volatile enabling operation in environments above ambient without solvent loss, so that operating life is not terminated prematurely because of this; elevated temperature of operation can facilitate the catalysis of reactive gases, so that equilibrium gas concentrations may be measured where required; response time to a change in gas concentration can be rapid (e.g. ~ 50 ms for a zirconia oxygen sensor in more than 1000 PPM O₂ at 700 °C); the sensor can be highly selective showing little interference from the presence of other gases; the potentiometric devices have a logarithmic response and can measure gas concentrations over an extremely wide range (10⁶–10⁻²⁵ Pa of O₂ with a zirconia-based electrolyte under appropriate conditions); alternatively the amperometric devices (based upon current measurement) deliver a linear response, which is preferable in some applications, and thus solid state devices are versatile and can be tailored to the

applications. On the other hand, elevated temperature of operation can be a disadvantage so that, for example, an oxygen sensor operating at 700 °C may require the addition of a flame trap to prevent the ignition of potentially explosive mixtures of gases.

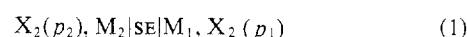
Oxygen sensors are widely used at the present time for controlling the air–fuel (A/F) ratio in combustion processes. Examples include detecting the stoichiometric point for the operation of a three-way catalyst in internal combustion engines and controlling fossil-fuelled boilers for maximisation of thermal efficiency while minimising the generation of carbon monoxide.

In the near future oxygen sensors are likely to be used to control the air–gas ratio in fully premixed condensing domestic boilers; if excess air levels are reduced the dew point of water vapour in the flue is raised so that the recovery of latent heat by condensation is increased.

2. Potentiometric sensors

2.1. General

Following Fouletier (1982/3) the potentiometric solid electrolyte gas sensor can be depicted as follows:



M₁ and M₂ are electronic conductors and act as cell electrodes to which electrical connections may be made; the solid electrolyte (SE) should be physically impervious to the gas X₂ which is at partial pressures p₁ and p₂; the electrolyte usually has a mobile ion which is a charged species of the gaseous atom, e.g. O₂/O²⁻, but this is not always the case. The electrode reaction (for the case involving an anion) is



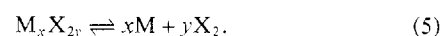
The EMF of cell (1) assuming reversibility is given by

$$E = (RT/nF) \int_{p_2}^{p_1} t_{ion} d \ln p. \quad (3)$$

t_{ion} is the transport number of the mobile ion while R, T and F have their usual significance. The electrolytes generally chosen have a very low electronic transport number under the conditions of operation, so that t_{ion} is close to unity. Equation (3) then becomes

$$E = (RT/nF) \ln(p_1/p_2). \quad (4)$$

Hence if p₂ is known (reference gas) then p₁ may be determined from a measurement of E (at a given T). The reference gas may originate from a gaseous source, e.g. ambient air or a gas cylinder, or may be generated from a solid as follows:



For a stoichiometric solid the equilibrium pressure of $X_2(p_2)$ is a monotonic function of temperature.

2.2. Effect of temperature

The variation of EMF with sensor temperature will now be derived in terms of standard thermodynamic functions. This analysis is based upon a previous discussion by Heyne (1978). The reader is referred to any standard text on physical chemistry for the background, e.g. Moore (1972).

The EMF of an electrochemical cell is given by

$$nFE = -\Delta G. \quad (6)$$

ΔG is the free energy change for the passage of n faradays of charge through the cell. The Gibbs–Helmoltz relation may be written

$$d\Delta G/dT = -\Delta S \quad (7)$$

where ΔS is the consequent change in the entropy of the system. Thus

$$dE/dT = -\Delta S/nF. \quad (8)$$

This indicates that the temperature coefficient of the EMF is proportional to the entropy change. Where a gaseous reference is employed (assuming ideal behaviour)

$$\Delta S = -R \ln(p_1/p_2) \quad (9)$$

and

$$dE/dT = -(R/nF) \ln(p_1/p_2), \quad (10)$$

which could, of course, have been derived directly from equation (4). Equation (10) reveals that the sensor has a temperature coefficient close to $0.2/n$ mV K^{-1} per decade ratio between the sample and reference gas pressures. In an oxygen sensor using the commonly employed air reference ($p_2 = 21$ kPa), temperature coefficients of approximately 0.5 and 1.0 mV K^{-1} are anticipated at 10^{-5} and 10^{-15} Pa partial pressure of oxygen in the sample gas respectively.

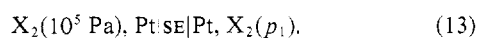
Consider now the following cell incorporating the solid reference M_xX_{2y} , that dissociates according to equation (5)



It is readily shown by summing the contributions of the two cells



and



that the temperature differential of cell (11) is given by

$$dE/dT = -\frac{1}{nF} \left(\frac{x}{y} S_M^0 - \frac{1}{y} S_{M_xX_{2y}}^0 + S_{X_2}^0 - R \ln p_1 \right) \quad (14)$$

where S^0 represents the standard entropy of the species shown as subscript. The relative magnitudes of the terms in equation (14) for a number of solid oxides (Kubaschewski and Alcock 1979) are shown in table 1. $(x/y)S_M^0$ and $(1/y)S_{M_xO_{2y}}^0$ are of similar magnitude and tend to cancel. The term $S_{O_2}^0$ is large (205 J K^{-1} mol $^{-1}$) and amounts to approximately 0.5 mV K^{-1} ; it is this term that results in the inevitably high temperature coefficient of cells containing a solid reference (Maskell and Steele 1986). The final term in equation (14), $-R \ln p_1$, is the same as that found in the cell with a gaseous reference (equation 10) and contributes 0.05 mV K^{-1} per decade ratio between p_1 and 10^5 Pa pressure. The signs of $S_{O_2}^0$ and $-R \ln p_1$ are the same (for $p_1 < 10^5$ Pa) and hence the contributions are additive.

This analysis has shown that the temperature coefficient of a cell with a gaseous reference is not large and can, if practicable,

Table 1. Thermodynamic data for some solid oxides at 298 K.

Oxide M_xO_{2y}	ΔS_1^\dagger (cal K^{-1} mol $^{-1}$) ‡	$\Delta S_2/4F^\ddagger$ (mV)
Bi ₂ O ₃	-6.1	0.46
CoO	-10.9	0.41
Cr ₂ O ₃	-5.4	0.47
Cu ₂ O	-12.8	0.39
FeO	-15.1	0.37
IrO ₂	-5.0	0.48
NiO	-3.9	0.49
OsO ₂	-4.6	0.48
PbO	-0.6	0.52
PdO	-0.7	0.52
ReO ₂	(2.5)	(0.56)
RuO ₂	-0.9	0.52
Ta ₂ O ₅	-5.7	0.47
ZnO	-1.0	0.52

$$^\dagger \Delta S_1 = (x/y)S_M^0 - (1/y)S_{M_xO_y}^0$$

$$^\ddagger \Delta S_2 = \Delta S_1 + S_{O_2}^0 (S_{O_2}^0 = 49 \text{ cal } K^{-1} \text{ mol}^{-1}).$$

$$§ 1 \text{ cal } K^{-1} \text{ mol}^{-1} = 4.184 \text{ J } K^{-1} \text{ mol}^{-1}.$$

be minimised by choosing p_2 to be similar to p_1 : the coefficient of a cell with solid reference, on the other hand, is always higher by ~ 0.5 mV K^{-1} (for $p_1 < 10^5$ Pa). This means that cells of the latter type require more precise temperature control than those with a gaseous reference for comparable precision of measurement.

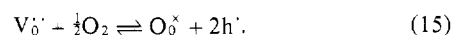
2.3. Response time

2.3.1. General principles. The EMF of a potentiometric cell is given by

$$E = (RT/nF) \int_{p_2}^{p_1} t_{ion} d \ln p. \quad (3)$$

If t_{ion} varies through the electrolyte then the observed EMF will depend upon the profile of t_{ion} against z where z is the distance from one interface. This effect has been considered in detail by Heyne and den Engelsen (1977): they showed that in general the effect was important with regard to the long-term drift of the EMF but had little influence on the short-term response time. Also, by careful preparation of the solid electrolyte, in particular eliminating as far as possible second phases with ionic transport numbers different from the main bulk phase, drift can be minimised.

Variations in ionic transport number within the ceramic arise as follows. Electronic defects are generated at high and intermediate gas pressures in an oxygen-ion conductor by the following process (shown in Kroger–Vink notation)



Clearly, the hole (h^{\bullet}) concentration is related to the oxygen partial pressure. A high hole concentration results in a significant electronic transport number so that t_{ion} is depressed below unity.

An important point arises from the above paper with regard to rate of response. Consider a system initially at equilibrium: it has an established t_{ion} against z profile. Let the sample gas pressure be changed rapidly to a different value. Equation (3) indicates that the EMF of the cell should change instantaneously to a new value because E is only governed by p_1 and p_2 and by the t_{ion} against z profile. The profile will change only slowly (for

$t_{\text{ion}} \neq 1$) as diffusion processes in the solid phase are slow and this will produce the long-term drift mentioned above.

In fact the response is not instantaneous because of the omission of a number of factors as listed below and discussed in detail in the appendix.

(i) The double layer at the electrode–electrolyte interface acts as a capacitor requiring the transfer of charge when the sensor EMF responds to a change in oxygen pressure.

(ii) The electrode potential cannot stabilise until the stoichiometry of the electrolyte in the double layer has achieved equilibrium with the gas phase.

(iii) Changes in stoichiometry throughout the electrolyte result in overvoltages due to charge transfer and perturbation of the oxygen partial pressure at the gas–solid interface.

(iv) A low electrode resistance to charge transfer reduces the response time of the sensor.

(v) The hydrodynamics in the gas phase influence the rate at which a p_{O_2} change in the bulk gas is transmitted to the sensor interface.

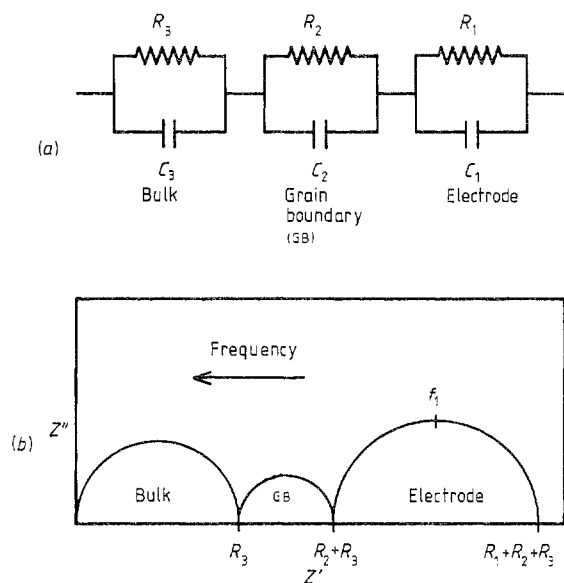


Figure 1. (a) Equivalent circuit representation of a sensor. (b) Complex plane impedance response of a sensor. The zenith of the electrode semicircle occurs at frequency f_1 .

2.3.2. Impedance analysis. In order to analyse its electrical behaviour, the gas sensor can be represented by the equivalent circuit shown in figure 1(a) (Bauerle 1969). The components R_1/C_1 , R_2/C_2 and R_3/C_3 are associated with the electrode, the grain boundaries and the grain interiors in the ceramic respectively. The AC spectrum for such a circuit plotted in the complex plane is shown in figure 1(b) with frequency of the applied signal, f , increasing from right to left. Z' and Z'' represent the in and out of phase components of the complex impedance respectively. The present discussion is only concerned with the processes indicated at the lowest frequencies associated with the electrode: typically the frequency range is 100 Hz and below. The point shown at the zenith of the electrode semicircle occurs at a frequency f_1 , such that

$$2\pi f_1 C_1 R_1 = 1 \quad (16)$$

Consequently the time constant for the electrode process is $(2\pi f_1)^{-1}$. A typical value for f_1 at 700 °C is 10 Hz (Kleitz *et al* 1981) corresponding to a time constant of less than 20 ms.

In a recent work (Verkerk and Burggraaf 1983) more complex equivalent circuits have been proposed for the electrode

processes involving Warburg impedances. These are introduced to account for diffusional processes that result in additional features in the impedance spectrum. Such processes might include the diffusion of oxygen atoms on the electrode or electrolyte surfaces or diffusion of electronic holes in the ceramic.

The impedance technique, by allowing separation of the various components of the sensor impedance, can provide a valuable insight into the factors controlling the response of the sensor. Note that deviation of the electrode impedance from a perfect semicircle indicates that the product RC is effectively varying and would result in a response curve deviating from that based on the simple theory where RC is taken as constant (Fewkes and Yarwood 1956).

2.3.3. Experimental data. In this section only work in non-reactive gases is considered, i.e. in O_2 –inert gas (e.g. Ar or N_2) mixtures.

(i) *Step changes in oxygen partial pressure.* Anderson and Graves (1982) applied a p_{O_2} step to a zirconia sensor and observed the resulting EMF change. They found the response times to be an order of magnitude greater than suggested from the electrical response to a small current pulse: this suggests that transport processes in the gas phase were a controlling influence. The EMF responses in going from high-to-low and from low-to-high p_{O_2} were compared and showed an asymmetry. However, when EMF values were converted to indicated p_{O_2} using equation (4), the asymmetry disappeared. This again was compatible with gas-phase diffusion control. Response time on a $\text{ZrO}_2\text{--Y}_2\text{O}_3$ electrolyte with a Pt electrode was typically ~ 1 s at 600 °C for a 90% change in sensor EMF compared with the equilibrium values.

Fouletier *et al* (1974) carried out response measurements in which oxygen pressure changes were induced by connecting two vessels containing gases of the same composition but at different pressures and obtained data obeying the following relationship

$$\Delta E = \Delta E_0 \{1 - \exp[-(t/\tau)^{1/2}]\} \quad (17)$$

where ΔE and ΔE_0 are the EMF changes after times t and infinity. The parameter τ displayed Arrhenius behaviour and the activation energy, E_A , was determined from the response time t_r (proportional to τ) using the empirical equation

$$t_r = A_1 p_m^{-1/2} \exp(-E_A/RT) \quad (18)$$

where A_1 is a constant and p_m the mean pressure: i.e.

$$p_m = \frac{1}{2}(p_{\text{initial}} + p_{\text{final}}). \quad (19)$$

Both Pt and Ag electrodes responded according to equation (18) but with different A_1 and E_A parameters: the response of the Ag electrodes was faster than that of the Pt electrodes. At 500 °C the response times for a 99% change in sensor EMF were 100 s and 3 s for Pt and Ag electrodes respectively on a $\text{ZrO}_2\text{--Y}_2\text{O}_3$ electrolyte.

The dependence of t_r on $p_m^{-1/2}$ may have been significant, as other studies (Bauerle 1969, Kleitz *et al* 1981, Verkerk *et al* 1983) have shown the electrode resistance on zirconia-based electrolytes to display an inverse square root dependence on p_{O_2} . For a constant value of the double layer capacitance, the RC time constant would be expected to increase with decreasing p_{O_2} in accordance with equation (18).

Recently response measurements on a variety of systems, using relatively high gas flow rates onto the electrodes to minimise gas phase diffusion limitations, have been reported (Winnubst *et al* 1985). Results were found to be consistent with equations (17) and (18) for times longer than 0.5 s. The response was probably controlled by gaseous diffusion at times less than 0.5 s. Interestingly, Fouletier *et al* (1974) measured t_r for

$\Delta E/\Delta E_0$ values of 0.99. Consequently measurements were made at sufficiently long times that gas-phase diffusion was, presumably, no longer a controlling factor.

Some of the results of Winnubst *et al* (1985) are shown in figure 2. Response times were determined for 10–90% response and showed several interesting features: in particular, under the conditions of the work, the response of electrodes on ZrO_2 -based electrolytes was faster than on Bi_2O_3 -based materials; also a Au electrode showed superior performance to Pt.

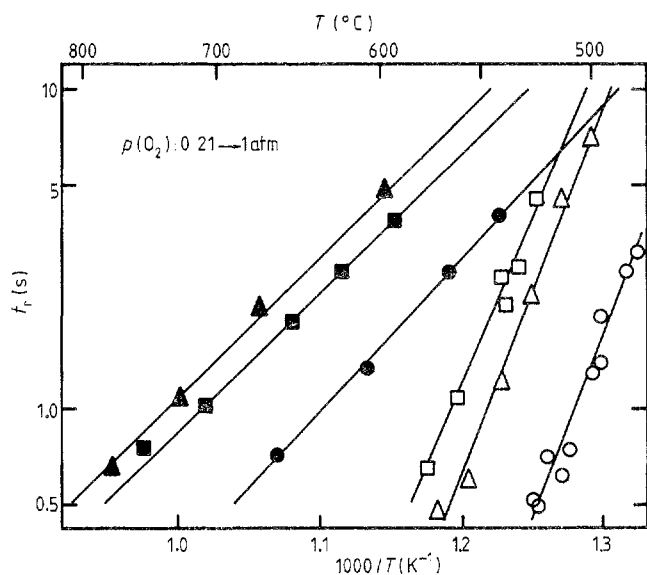


Figure 2. Response time as a function of temperature for stabilised ZrO_2 - and Bi_2O_3 -based electrolytes. Composition (mol %): Δ , 83 ZrO_2 -17 $YO_{1.5}$; \square , 79 ZrO_2 -21 $YO_{1.5}$; \bullet , 80 Bi_2O_3 -20 Er_2O_3 ; \blacksquare , 70 Bi_2O_3 -30 Er_2O_3 ; \blacktriangle , 60 Bi_2O_3 -40 Er_2O_3 . Pt electrodes were used for all cases except \circ , where Au was used (Winnubst *et al* 1985). ($p(O_2)$: 21–100 kPa. (Diagram courtesy Chapman and Hall Ltd, London.)

(ii) *Impedance measurements.* In pioneering work employing the AC technique Bauerle (1969) postulated that the electrode semicircle (figure 1(b)) resulted from the resistance to the electrode reaction (R_1) and the double layer capacitance (C_1): this has become generally accepted with minor modifications. Wang and Nowick (1979) observed a frequency dependence of R_1 and C_1 with CeO_2 -based electrolytes and proposed that diffusional processes were influencing the behaviour requiring the addition of a Warburg impedance to the equivalent circuit. Verkerk and Burggraaf (1983) refined the analysis and made the following observations. On zirconia-based electrolytes the impedance spectra could be fully explained in terms of the dissociative adsorption of oxygen onto Pt electrodes and the diffusion of oxygen atoms to the three-phase boundary. With Bi_2O_3 -based electrolytes, on the other hand, a dominant Warburg impedance appeared to be associated with a diffusional process within the bulk of the electrolyte. It was speculated that the rate-determining process involved the transport of holes (h^\cdot).

These findings aid the understanding of the slow response of electrodes on Bi_2O_3 -based electrolytes (§ 2.3.3.(i)) and the following is a possible explanation. In response to a change in oxygen partial pressure the stoichiometry of the Bi_2O_3 adjusts (§ 2.3.1.(ii)) and this involves the diffusion of holes (and complementary transport of V_o^\cdot) throughout the bulk of the electrolyte. This retards the response because the achievement of a stable electrode potential requires the double layer region to come to equilibrium with the gas phase. The diffusion of holes to

the surface may also induce a significant overpotential on the electrode.

(iii) *Influence of electrode material.* The work of Fouletier *et al* (1974) and of Winnubst *et al* (1985) has demonstrated that the sensor response can be improved by employing either Au or Ag rather than Pt as electrode material. Fouletier *et al* (1976) recorded that Kleitz (1968) had found the overpotential on Ag electrodes to be lower than on Pt electrodes. Issacs and Olmer (1982), on the other hand, reported lower currents on Au compared with Pt for a given overpotential. Badwal *et al* (1984) found the relaxation times for urania-scandia electrodes to be one or two orders of magnitude shorter than those for Pt electrodes under similar conditions.

Clearly there is scope for improving the response of oxygen sensors by optimising the electrode composition and structure. Such developments will benefit from further work aimed at improving our understanding of the role of the electrode in the oxygen reaction and identifying rate-determining steps and sources of capacitance. The importance of this work lies in developing sensors that retain acceptable response times while operating at lower temperatures.

2.4. Reactive gases

2.4.1. *General formulation of the model.* Only situations involving non-reactive gases have been discussed so far in this review (e.g. O_2 in Ar). In practical conditions reactive gases, i.e. gases not in thermodynamic equilibrium, are often encountered and the response of gas sensors to such mixtures must be considered. Reactive gases sometimes contain a plethora of active components, but such mixtures are too complex to model satisfactorily. Fortunately, a relatively small number of components generally has an overriding influence allowing a tractable yet meaningful analysis to be achieved.

The scheme described below is based upon that presented by Anderson and Graves (1981) but has been generalised to apply to a three-component system containing gases A, B and C that interact according to the reaction



The species reach the electrode surface from the bulk gas by diffusion and because the diffusion layer may be poorly defined or complex it is referred to as a boundary layer. In order to model the system so that qualitative and possibly quantitative predictions may be made, the transport and reaction equations must be set up as shown below. In this model it is assumed that homogeneous reaction in the gas phase does not occur. The gases A, B and C may be monatomic, diatomic etc or monomeric, dimeric etc and thus are written as A_a , B_b , C_c where a , b and c represent the number of the components A, B and C in each molecule. The first three equations quantify surface reactions and state that the rate of change in fractional surface coverage of a species i , θ_i , depends upon the adsorption and desorption and the forward and reverse rates of reaction. In all cases isothermal Langmuir-type kinetics are assumed

$$d\theta_A/dt = -ak_2\theta_A^a + ak_A p_A \theta_v^a - xk_R \theta_A^x \theta_B^y + xk_D \theta_C^z \theta_v^{x+y-z} \quad (21)$$

$$d\theta_B/dt = -bk_4\theta_B^b + bk_B p_B \theta_v^b - yk_R \theta_B^y \theta_A^x + yk_D \theta_C^z \theta_v^{x+y-z} \quad (22)$$

$$d\theta_C/dt = -ck_6\theta_C^c + ck_C p_C \theta_v^c + zk_R \theta_A^x \theta_B^y - zk_D \theta_C^z \theta_v^{x+y-z} \quad (23)$$

The next three equations quantify rates of transport from the bulk gas across the boundary layer to the electrode surface

$$dp_A/dt = -k_1(p_A - p'_A) - k_A p_A \theta_v^a + k_2 \theta_A^a \quad (24)$$

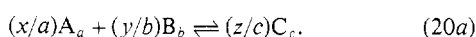
$$dp_B/dt = -k_3(p_B - p'_B) - k_B p_B \theta_v^b + k_4 \theta_B^b \quad (25)$$

$$dp_C/dt = -k_5(p_C - p'_C) - k_C p_C \theta_v^c + k_6 \theta_C^c \quad (26)$$

where p_A , p_B and p_C are the partial pressures of A, B and C respectively adjacent to the electrode surface; p'_A , p'_B and p'_C refer to pressures in the bulk; θ_v is fractional surface coverage by vacancies; k_1 , k_3 and k_5 are the mass transfer coefficients between the bulk gas and boundary layer; k_A , k_B and k_C are the adsorption rate constants for the subscript species while k_2 , k_4 and k_6 are the desorption rate constants; k_R and k_D are the forward and reverse rate constants for the surface reaction.

The difficulty of the task is now apparent in this considerably simplified model. For example, only reactions between adsorbed gas atoms or molecules is considered whereas reaction between an adsorbed species and a gaseous species also is also possible. Further, only chemical reaction between A and B is allowed for and electrochemical redox reactions are ignored. Notwithstanding this, the analysis can provide a valuable insight into the processes occurring at the electrode-electrolyte interface.

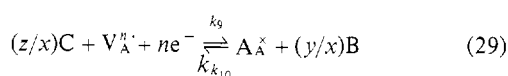
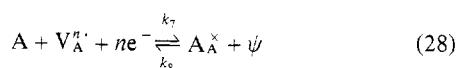
The rate constants in equations (21)–(26) are related by the equilibrium constant, K_{eq} , for the reaction



Thus

$$K_{eq} = \left(\frac{ak_2}{k_A} \right)^{x/a} \left(\frac{bk_4}{k_B} \right)^{y/b} \left(\frac{ck_6}{k_C} \right)^{-z/c} \frac{k_D}{k_R} \quad (27)$$

In principle, at this stage, if the rate constants, mass transfer coefficients and the equilibrium constant are known then the surface coverages θ_A , θ_B and θ_C may be determined for given bulk gas pressures. These theta values then determine the electrochemical potential of the electrode or the sensor EMF, as shown below. In the relatively simple scheme being considered the observed voltage is a consequence of the following two reactions



where ψ represents a vacant surface site. The observed voltage is a mixed potential, as shown in figure 3. The anodic current of one reaction is equal in magnitude to the cathodic current of the other so that the net current is zero. In the special case where the reactants A and B are in thermodynamic equilibrium with the product then $E_1 = E_2 = E_{mixed}$. An alternative and equivalent scheme is to invoke reaction rate theory (Anderson and Graves

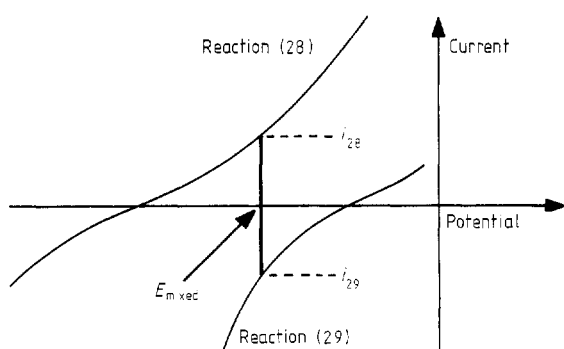


Figure 3. Formation of a mixed potential between reactions (28) and (29) at E_{mixed} where the net current is zero, i.e. $i_{28} + i_{29} = 0$.

1981), which leads to an expression for the mixed potential ϕ :

$$\phi = \frac{RT}{nF} \ln \left[\frac{k_7}{k_8} \left(\frac{(\theta_A/\theta_v) + (k_9/k_7)(\theta_C^{z/x}/\theta_v)}{1 + (k_{10}/k_8)(\theta_B^{y/x}/\theta_v)} \right) \frac{w}{A_s} \right] \quad (30)$$

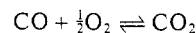
where w and A_s are the surface concentrations of V_A^n and A_A^x respectively; taking these as identical on the sample and reference sides of the electrolyte the potential of the reference ϕ' is given by

$$\phi' = \frac{RT}{nF} \ln \left[\frac{k_7}{k_8} \left(\frac{\theta_A}{\theta_v} \right) \frac{w}{A_s} \right] \quad (31)$$

and the cell EMF is

$$\Delta V = \phi - \phi' = \frac{RT}{nF} \ln \left[\left(\frac{(\theta_A/\theta_v) + (k_9/k_7)(\theta_C^{z/x}/\theta_v)}{1 + (k_{10}/k_8)(\theta_B^{y/x}/\theta_v)} \right) \left(\frac{\theta_v}{\theta_A} \right) \right] \quad (32)$$

2.4.2. Application of the model to oxygen sensing. Combustion systems and in particular the exhaust of internal combustion engines contain a variety of hydrocarbons (Fleming 1977). CO and H_2 comprise less than a few per cent of the total exhaust gas but they are ten times more abundant than all other hydrocarbons. Fleming gives a number of reasons why CO, rather than H_2 , has the principal influence on cell EMF. Also Haaland (1980) found H_2 to be very readily oxidised with evidence of substantial homogeneous oxidation at 700 °C. Thus most work has considered the reaction



to be the most important in determining the EMF of oxygen sensors when exposed to reactive gases.

Anderson and Graves (1981) employed numerical techniques to solve equations (21)–(32) involving substituting selected values for the unknown rate constants. In all cases k_9 and k_{10} were set equal to zero on the basis of insufficient knowledge of their relative values: Heyne (1978) in a much simpler treatment also did this to facilitate the analysis. In effect it is equivalent to ignoring reaction (29) so that the potential ϕ is no longer a mixed potential but is controlled totally by the oxygen reaction (28). This might be expected to lead to considerable errors for O_2/CO ratios of less than 0.5 where reaction (29) should be dominant. Hence, the predicted characteristics in the rich region must be viewed with caution when employing this assumption.

Some of the results of the numerical analysis of Anderson and Graves are presented below. Figure 4 shows the situation where mass transport is fast. As expected (curve A), when there is negligible surface reaction the sensor detects the total bulk oxygen and does not respond to changes in the O_2/CO ratio: this is the equivalent of sensing CH_4/O_2 on Ag. In curve C the surface reaction is fast and the behaviour is similar to the theoretical curve D, which corresponds to thermodynamic equilibrium.

Figure 5 shows the influence of mass transfer rate. In curve A mass transfer is fast but different adsorption rates of CO and O_2 are assumed: the deviation from the theoretical equilibrium curve is substantial as was predicted by Heyne's analysis (1978). Curves B and C represent progressively slower mass transfer and the result is now close to the theoretical equilibrium curve. This illustrates very well the important finding that for gases with similar transfer coefficients (such as O_2 and CO) the position of the potential step should correspond reasonably well with the theoretical equilibrium result, provided mass transfer rates are slow.

However, the analysis predicts substantial deviations from the theoretical equilibrium curve when mass transfer is slow and

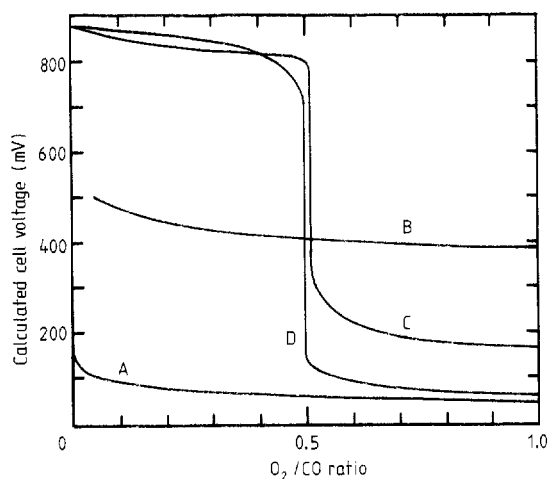


Figure 4. Calculated sensor EMF against bulk O_2/CO ratio assuming rapid mass transfer to the sensing electrode. A, slow surface reaction (k_R and k_D small); B, intermediate situation; C, rapid surface reaction (k_R and k_D large); D, equilibrium curve. (Anderson and Graves 1981). (Reprinted by permission of the publisher, The Electrochemical Society, Inc.)

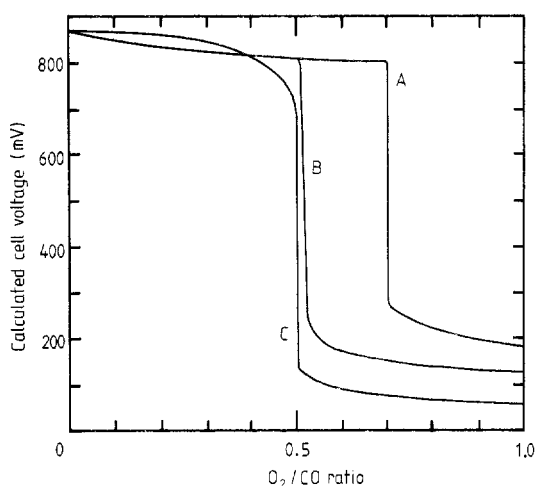


Figure 5. Calculated sensor EMF against bulk O_2/CO ratio assuming dissimilar adsorption rates of O_2 and CO . A, rapid mass transfer; B, intermediate situation; C, slow mass transfer (Anderson and Graves 1981). (Reprinted by permission of the publisher, The Electrochemical Society, Inc.)

the mass transfer coefficients of the reacting gases differ: the latter vary as $M^{-1/2}$ where M is the molecular weight of the gas. Thus, mass transfer coefficients for O_2 and H_2 differ by a factor of four whereas for O_2 and CO the ratio is 1.07.

2.4.3. Experimental results. The EMF of a zirconia sensor with an air reference was monitored against the ratio of combustible gas to oxygen for four oxidisable gases by Takeuchi *et al* (1978). Their results, shown in figure 6, were in close accord with the numerical analysis of Anderson and Graves, showing a linear relationship between λ_C (the λ value at which the potential step was observed) and the diffusion coefficient of the combustible gas.

Interestingly, Anderson and Graves (1981) found the potential step for O_2/CH_4 mixtures to occur at an anomalously low λ_C value when using a Pt electrode indicating the difficulty of fully catalysing the oxidation of CH_4 .

In practice exhaust systems are not as far from equilibrium as the one in the above laboratory measurements and major deviations of λ_C from unity would not, in general, be anticipated.

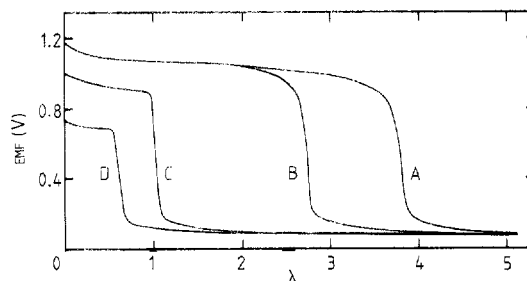


Figure 6. Experimentally determined EMF of a zirconia sensor for various gas mixtures. A, $H_2-O_2-N_2$; B, $D_2-O_2-N_2$; C, $CO-O_2-N_2$; D, $C_4H_{10}-O_2-N_2$. λ is the actual oxygen to reductant ratio compared with the stoichiometric oxygen to reductant ratio (Takeuchi *et al* 1978; this paper was originally presented at the 1978 Fall Meeting of The Electrochemical Society, Inc. held in Pittsburgh, PA).

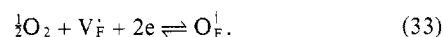
2.5. Selectivity

The response of the sensor to reactive gases is dependent upon the choice of electrode material. In many applications, such as combustion control, the required oxygen measurement is usually that pertaining to thermodynamic equilibrium: in such cases Pt is normally the preferred choice of electrode material because of its high catalytic activity. However, there are other situations where the actual O_2 content of a reactive gas mixture is required. Sandler (1971) found that in CH_4/O_2 mixtures Ag showed negligible catalytic activity and responded only to the total O_2 content of the mixture. Haaland (1980) confirmed this result and investigated a number of electrode materials in various reactive gas mixtures. He found that Ag deposited on Pt was non-catalytic while Au was only slightly catalytic. Pt poisoned with lead was particularly non-catalytic above 500–550 °C. A possible problem with this electrode is the introduction of the Pb–PbO couple into the electrode. This would be expected to result in slow response particularly when sweeping the oxygen pressure through the value at which the Pb–PbO couple is in equilibrium (see figure 6 of Maskell and Steele 1986).

Solid electrolyte sensors are normally considered to be highly selective because the ceramic may be chosen with a single mobile anion, e.g. A^{n-} and thus only the gas A_n or gases that can take part in a redox equilibrium with A e.g.



are expected to influence the sensor EMF. In most cases this is true but there are exceptions. For example, O_2 may be sensed using a fluoride electrolyte (Ramanarayanan *et al* 1979, Siebert and Fouletier 1983, Kumata *et al* 1984). This is probably the result of oxygen ions being inserted into fluoride vacancies



2.6. Blocking

The foregoing discussion has assumed electrode reversibility. However, if a species is very strongly adsorbed onto the electrode surface it can block sites for adsorption so that the electrode is no longer fully reversible towards the gas being sensed. It appears that this situation can arise with CO on Pt at relatively low temperatures (< 500 °C). Referring back to figure 4 and equations (28) and (29) it is clear that if most of the adsorption sites are blocked by CO then the O_2/O^{2-} reaction cannot contribute to the mixed potential. Further, the θ_{CO} term (θ_B in equation 30) dominates so that ϕ and ΔV (equation 32) assume very negative values compared with those expected for a reversible system. This may account for the large anomalous

EMF deviations previously reported (Fouletier 1982/3, Mogab 1973, Pizzini 1973). Where this occurs it can often be alleviated by raising the cell temperature, which results in desorption of much of the strongly bound CO.

2.7. Degradation of performance

The performance of oxygen sensors deteriorates with time. This may involve either the degradation of the ceramic or of the electrodes or both. The former aspect has been discussed previously (Steele *et al* 1981, Maskell and Steele 1986). Electrodes may degrade for a number of reasons.

(i) At high operating temperatures (e.g. > 800 °C with Pt) a porous metallic electrode tends to sinter with a consequent decrease of surface area and concomitant reduction of the length of the three-phase boundary. These changes reduce the exchange current density on the electrode and its catalytic activity, and response may become sluggish.

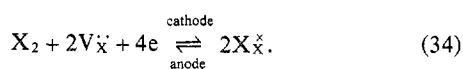
(ii) When operating in atmospheres containing aggressive components, e.g. H₂S, SO₂, Pb, dust etc, the electrodes may take up these contaminants and become poisoned. In particular, as was discussed in § 2.5, H₂S or Pb compounds may reduce the catalytic activity of the electrode: poisoning by the former is partially reversible while poisoning by the latter is irreversible. This contamination can result in a sensor that records an oxygen content closer to the actual oxygen level rather than the equilibrium value (Fleming 1977).

3. Amperometric sensors

3.1. General theory

The discussion in this section is taken principally from the work of Dietz (1982).

A schematic diagram of the limiting-current sensor is shown in figure 7. The device is used to pump gas X₂ from the cathode to the anode, the processes occurring at the electrodes being



This equation assumes that X is divalent for simplicity but (34) may readily be transformed for alternative valency of the active species.

A porous barrier is fixed in front of the cathode to restrict transport of X₂ to the electrode. If a sufficient voltage is applied between the anode and the cathode then the partial pressure of X₂ at the cathode is reduced to a value close to zero. This is the limiting condition and the current flowing, *i*_{lim}, is controlled by the rate of diffusion of X₂ through the porous barrier according to Fick's first law,

$$i_{lim} = nFD(Q/L)c_{X_2} \quad (35)$$

n is the number of electrons transferred per molecule of X₂ (*n* = 4 for O₂ in equation (34)) and *D* is the diffusion coefficient; *Q* is the sum of the cross sections of the pores of effective length *L*; *c*_{X₂} is the concentration of X₂ in the sample gas. Equation (35) shows that the limiting current is proportional to the gas

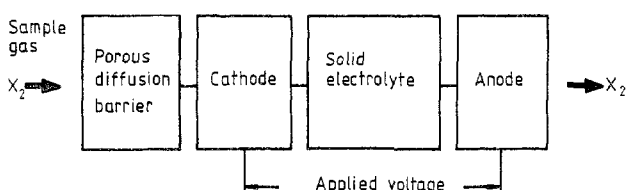


Figure 7. Schematic diagram of the limiting-current sensor. (Diagram courtesy North-Holland Physics Publishing, Amsterdam.)

concentration (compare equation (4) for the potentiometric device).

One of the problems involved in constructing practical devices is the very high diffusion coefficients of gases; e.g. *D*_{O₂} (in N₂) is 16 and 150 mm² s⁻¹ at 20 °C and 700 °C respectively. These values are four to five orders of magnitude higher than for O₂ in aqueous solutions. Consequently, diffusion barriers must restrict gases very severely, particularly since pump currents through solid electrolytes are restricted by the ionic conductivity of the ceramic. Dietz (1982) described various forms of diffusion barrier which were successfully employed for O₂ sensing.

The diffusion mechanisms of importance are bulk and Knudsen diffusion and the predominant type is dependent upon the pore size of the diffusion barrier. Bulk diffusion occurs where the pore size is larger than the mean free path (typically 10 μm at atmospheric pressure): Knudsen diffusion predominates for very small pores (e.g. ~ 10 nm). In the intermediate region both types of diffusion contribute to molecular transport.

Dietz (1982) has considered the effect of temperature and total gas pressure, *p*, on *i*_{lim} for both types of diffusion. For bulk diffusion the limiting current is proportional to both the mole fraction, *x*₁, of the active component X₂ and to *T*^{0.7} and is independent of *p*. For Knudsen diffusion *i*_{lim} is proportional to both *T*^{-0.5} and to *p**x*₁. It should be possible, by using a barrier with pores in the transition region between bulk and Knudsen behaviour, to obtain a characteristic showing little dependence upon temperature.

Characteristics of an amperometric oxygen sensor are shown in figure 8 (Dietz 1982) for O₂-N₂ mixtures. The limiting current plateau is clearly evident and *i*_{lim} is proportional to *x*_{O₂}.

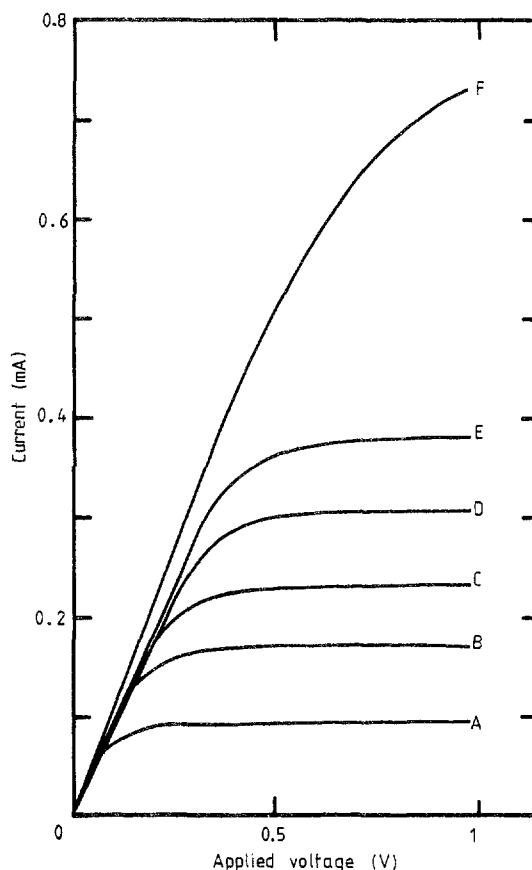


Figure 8. Characteristics of a limiting-current sensor where the diffusion barrier was a laser-drilled hole, 100 μm in diameter, filled with porous ceramic. Percentage of O₂ in N₂: A, 1; B, 2; C, 3; D, 4; E, 5; F, 10. (Dietz 1982). (Diagram courtesy North-Holland Physics Publishing, Amsterdam.)

3.2. Response time

The theoretical current–time characteristic, derived from data presented by Crank (1956), for the case where the limiting process is diffusion in the barrier adjacent to the cathode is shown in figure 9. A 90% response to a step change in p_{X_2} would be predicted for $t_{90} = 0.3 l^2/D$. Substituting in the typical values $l = 2$ mm, $D = 100$ mm² s⁻¹ reveals $t_{90} = 12$ ms. Thus the response is rapid and not likely to be rate-determining.

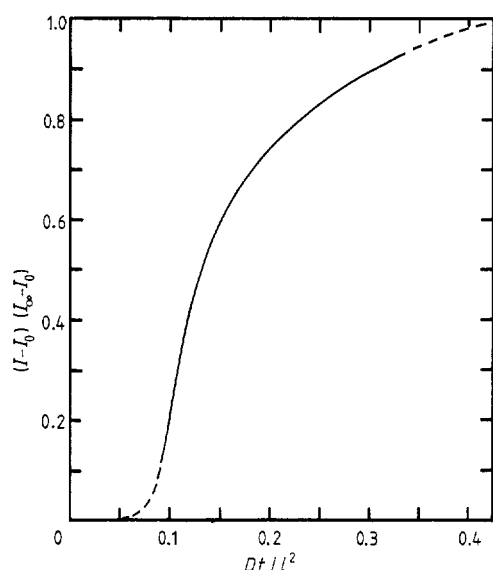


Figure 9. The theoretical response of a limiting-current sensor to a change in sample gas pressure when the diffusion barrier is controlling the behaviour. I , I_0 and I_∞ are the measured current at time t , at $t = 0$ and $t = \infty$ respectively, D is the diffusion coefficient and l the pore length.

3.3. Reactive gases

Very little has been reported in this area. Dietz, using Pt electrodes with O₂–CO mixtures (containing sufficient O₂ to allow conversion of all the CO to CO₂), found that the sensor measured the equilibrium oxygen value. However, it was not clear whether the diffusion barrier or the Pt electrode had catalysed the reaction.

When reducible gases other than O₂ are present in the sample gas then these may also contribute to the reduction current provided a sufficiently large overvoltage is applied to the cathode (Dietz 1982, Saji *et al* 1985). The reduction curves for H₂O and CO₂ occur in the same potential range and cannot be separated.

3.4. Degradation

Additional modes of deterioration compared with potentiometric devices relate to the diffusion barrier and result in progressive changes in characteristics. Two possible mechanisms that result in such changes are the following.

- (i) Blocking of pores in the barrier by dust in the sample gas.
- (ii) Structural changes of a porous ceramic. Dietz observed changes in devices employing a thin layer of ceramic (20–30 μm thick) applied over an electrode to produce a barrier with very low porosity.

3.5. Operating region

The amperometric oxygen sensor can only be used where the oxygen–reductant (or air/fuel) ratio is lean of stoichiometry. This is a serious limitation and arises because potentials are essentially referred to that of the anode in the sample gas. On passing through the stoichiometric point the anode potential

changes by more than 500 mV (see figure 8 of Maskell and Steele 1986). Typically the amperometric sensor is operated at 0.8 V. On passing through stoichiometry to $\lambda < 1$ (rich region) the overvoltage applied to the cathode is then approximately 1.3 V (relative to an air reference) and this is now sufficiently cathodic to reduce CO₂ and H₂O resulting in current flow (Saji *et al* 1984). However, there is no indication to the user that the system is now sub-stoichiometric and the current might be interpreted as indicating an oxygen surplus (i.e. $\lambda > 1$). This problem can be solved by using the pump-gauge devices discussed in § 5.

4. Coulometric sensors

In coulometry a given volume of gas is quantitatively converted by electrolysis and the partial pressure determined from the charge passed. There are many ways of performing such a measurement but the one described below is sufficient to explain the principle. Heyne (1976) described the device shown schematically in figure 10. It comprises an electrochemical pump and a leak into an enclosed volume. Initially a constant current is applied to the pump to remove oxygen rapidly from the cavity much faster than its leakage rate through the aperture.

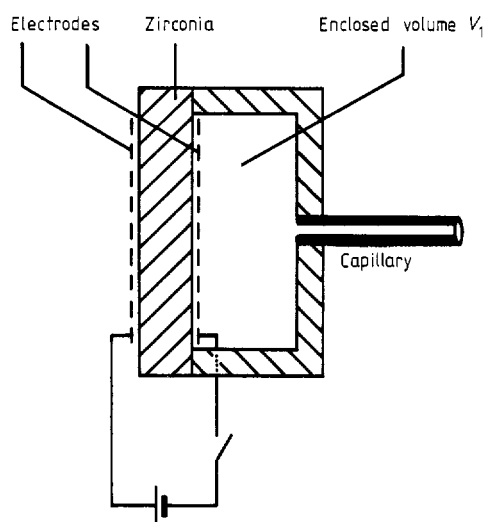


Figure 10. Coulometric sensor (Heyne 1976).

When almost all the oxygen is removed the voltage on the pump rises sharply. The current is then discontinued and a period follows during which oxygen leaks into the enclosed volume from the surrounding gas. This period is long enough so that the inner and outer gases closely approach equilibrium. The pump current is then re-applied and the cycle repeated. The oxygen partial pressure in the sample gas can be calculated by invoking Faraday's law as follows

$$p_1 = RTq/4FV_1 \quad (36)$$

where q is the charge passed and V_1 the enclosed volume. If the current applied is constant (I) then p_1 is given by

$$p_1 = RTIt_1/4FV_1. \quad (37)$$

The measured value t_1 is directly proportioned to the partial pressure, p_1 , which is an advantage in the lean region (compare the logarithmic response of the potentiometric sensor, equation (4)). Interestingly, unlike the amperometric sensor, the calibration is independent of the capillary characteristics and depends only upon I , V_1 and T . The sole requirement is that the waiting time is greater than the diffusion time which is much greater than

pumping time. Clearly the response time in this mode cannot be shorter than the cycle time.

5. Pump-gauge devices

5.1. General

These sensors employ appropriate ionic conductors in both the pumping (equation (34)) and sensing modes (equation (4)). Arrangements are shown schematically in figures 11(a) and (b). The device consists of an enclosed volume, V_1 , and two ionically conducting materials each in contact with both the internal and external gases with partial pressures of the gas to be sensed of p_2 and p_1 respectively. There may also be a pore or porous material connecting the inner and outer regions. These arrangements allow the measurement of p_1 via a number of operating modes as discussed below.

5.2. Coulometric

Haaland (1977) constructed a device of the type shown in figure 11(a) and operated it as an oxygen sensor as follows. The device was placed into the sample gas of unknown oxygen partial pressure. Oxygen was electrochemically pumped out of the volume V_1 until the gauge EMF, E , reached a sufficiently high value to indicate that p_2 was close to zero. (The EMF E is approximately 50 mV for each decade of the ratio of p_1/p_2 at 1000 K.) The current to the pump was then reversed and the charge passed, q , determined to achieve $p_2 = p_1$ ($E = 0$). This enabled calculation of p_1 according to equation (36)

$$p_1 = RTq/4FV_1. \tag{36}$$

If the magnitude of the applied current is constant then the pressure p_1 is proportional to the time of pumping and to T . Clearly the determination is intermittent and the response time cannot be less than the cycle time of the device. The latter may be reduced by minimising V_1 and maximising the pump current. Cells may be constructed with $V_1 < 1 \text{ mm}^3$ (Maskell *et al* 1987b).

The oscillatory mode of operation has been further developed by Hetrick *et al* (1982) and by De Jong (1983) using

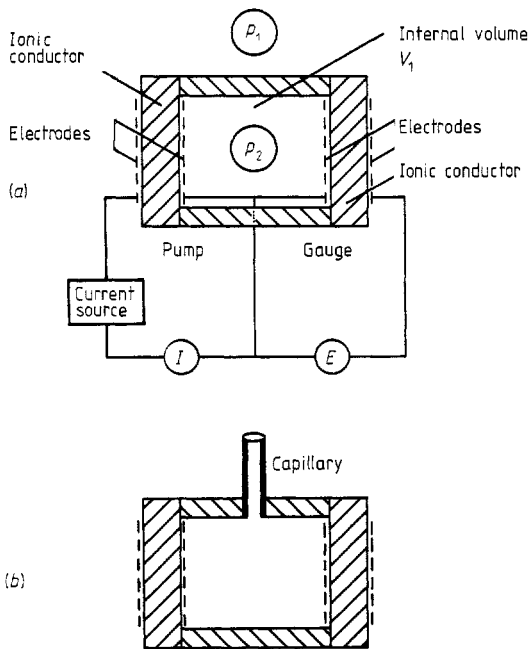


Figure 11. Pump-gauge devices. (a) internal volume totally sealed, (b) capillary joining inner volume with outer gas. Apart from capillary, devices (a) and (b) are identical.

cells of the type in figures 11(b) and (a) respectively. In this mode pumping may be carried out between any two predetermined gauge EMFs, E_Y and E_Z , in the range from -1 to $+1$ V although in practice normally of magnitude ≤ 100 mV. Thus the internal partial pressure is pumped between p_Y and p_Z respectively. Using equation (4)

$$p_Y = p_1 \exp(4FE_Y/RT) \tag{4a}$$

$$p_Z = p_1 \exp(4FE_Z/RT). \tag{4b}$$

The ideal gas equation may be applied:

$$p_Y - p_Z = \Delta n RT/V_1 \tag{38}$$

where Δn is the number of moles of gas pumped between the EMF values E_Y and E_Z and is related to the charge, Δq , by Faraday's law (assuming leakage rates to be small compared with the current): for a reaction involving 4 faradays/mole (e.g. oxygen reaction)

$$\Delta q = 4F\Delta n. \tag{39}$$

Simplifying the above equations,

$$p_1(\exp(4FE_Y/RT) - \exp(4FE_Z/RT)) = RTI\gamma/8FV_1 \tag{40}$$

where γ is the cycle time and I is the current. Equation (40) shows that for fixed E_Y and E_Z values, the cycle time, γ , is proportional to p_1 . In the particular case where $|E_Y|$ and $|E_Z| \ll RT/4F$ (i.e. $\ll 25$ mV) then the higher-order term in the exponentials may be ignored to reveal

$$p_1 = (RT/4F)^2 [I\gamma/2V_1(E_Y - E_Z)]. \tag{41}$$

This equation contains T to the second power indicating that attention must be paid to the control of temperature for accurate results. Interestingly where $E_Y = 0$ and $E_Z > 50$ mV, equation (36) is applicable and temperature control is less critical.

In the above discussion, as it relates to oxygen sensing, it has been assumed that the enclosed volume contains only oxygen as a reducible gas. This can be a reasonable assumption for the arrangement of figure 11(a) but not for that in figure 11(b). In the latter case this would result in uncertainty of the sample gas composition for the reasons presented in § 3.5.

5.3. Amperometric without fixed reference

The arrangement for this mode of operation is that shown in figure 11(b) with the circuit shown in figure 12 (Hetrick *et al* 1981). The pump current is automatically adjusted continuously to hold the gauge EMF at some predetermined value E_s .

$$E_s = (RT/4F) \ln(p_1/p_2). \tag{4c}$$

In the steady-state situation the current, I_p , is given by

$$I_p = 4F\sigma_L(p_1 - p_2) \tag{42}$$

where σ_L is the leak conductance of the diffusion barrier. It can be quantified for a cylindrical pore of cross-sectional area A_1 and length l

$$\sigma_L = DA_1/RTl. \tag{43}$$

Thus

$$I_p = 4F\sigma_L p_1(1 - \exp(-4FE_s/RT)). \tag{44}$$

For a given gauge EMF, E_s , the current is proportional to the oxygen partial pressure in the sample gas. Hetrick *et al* (1981) suggested that by an appropriate choice of E_s the temperature dependence of the sensor in this mode can be small.

Again this sensor is satisfactory in the region lean of stoichiometry but is inevitably deficient where a combustion system has the possibility of crossing stoichiometry into the rich region. This is a serious drawback for operation in boilers where

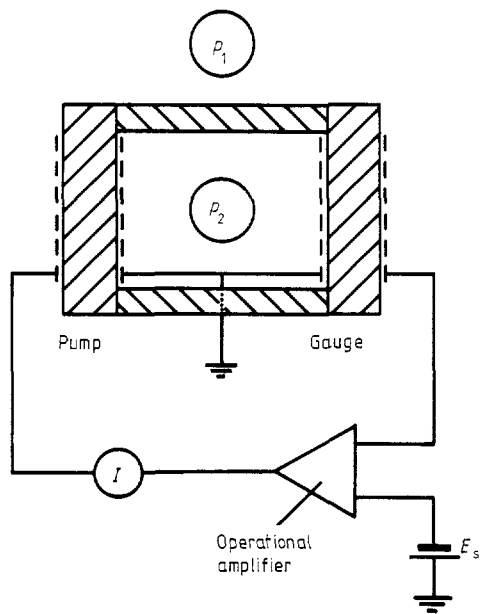


Figure 12. Circuit for operating the pump-gauge at a constant ratio of p_1/p_2 . The gauge EMF is automatically maintained equal to the reference voltage E_s by an appropriate pumping current.

it is essential that the A/F ratio is always maintained with excess air to minimise CO formation. This problem is solved by the devices discussed in the next section.

5.4. Amperometric with fixed reference

Dietz (1982) pointed out the advantage to be gained by providing a gas of fixed composition adjacent to the anode on a single two-electrode amperometric sensor (figure 7): traversal of stoichiometry then results in reversal of current flow so that the regions $\lambda < 1$ and $\lambda > 1$ are clearly identified.

With only a small increase in complexity, application of a fixed gaseous reference to the gauge of the pump-gauge provides a stable reference as negligible current need be carried by it. A schematic representation of this argument is shown in figure 13

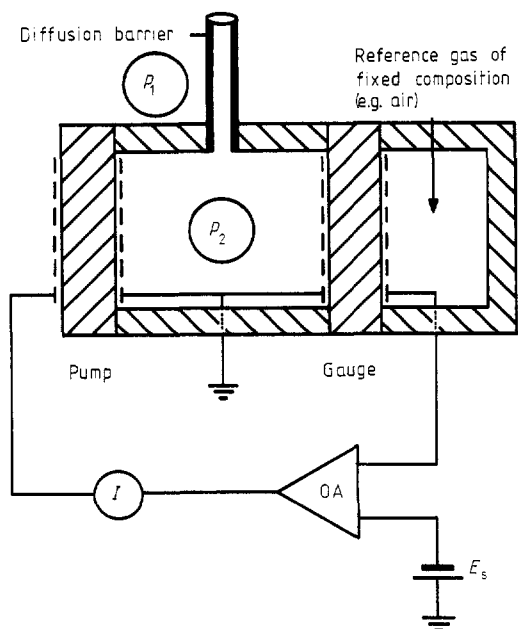


Figure 13. Amperometric pump-gauge with reference gas of fixed composition.

and has been translated into a practical device by Soejima and Mase (1985) with air as the reference gas. Some of their data are presented in figure 14 showing that the device can be used on both sides of stoichiometry by suitable choice of the working gauge EMF (i.e. 0.3–0.6 V).

A disadvantage of this arrangement is that a connection and suitable seal to the device must be provided to supply the reference gas.

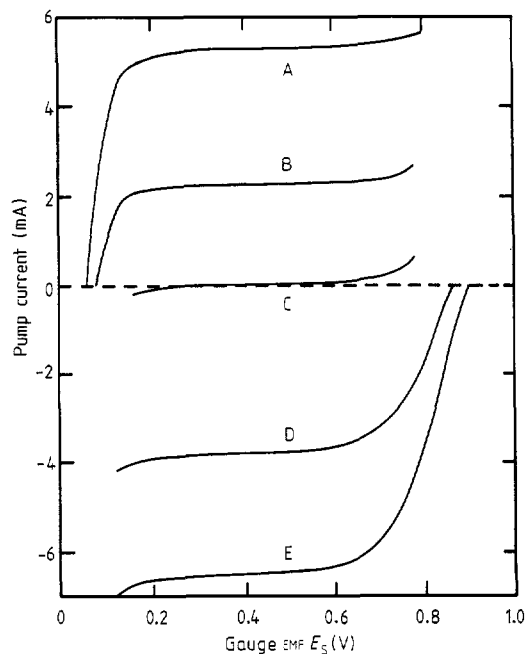


Figure 14. Characteristics of a cell of the type in figure 13 for various air/fuel ratios in a propane burner test. λ , A/F values: A, 1.6, 24; B, 1.23, 18; C, 1.0, 14.8; D, 0.89, 13; E, 0.82, 12 (Soejima and Mase 1985). (Reprinted with permission © 1985 Society of Automotive Engineers, Inc.)

5.5. Potentiometric with monitored internal reference

Maskell *et al* (1986) have described a novel mode of operation of a device of the type shown in figure 11(a). A sinusoidal current is applied to the pump and results in a sinusoidal variation of the internal reference gas pressure. This, in turn, leads to a pseudo-sinusoidal variation of the gauge EMF superimposed upon the potentiometric EMF resulting from the ratio of the external and mean internal oxygen partial pressures.

For a net applied current, I , given by

$$I = A_2 \sin \omega t \tag{45}$$

it has been shown (Maskell *et al* 1987b) that the gauge EMF is

$$E = \left(\frac{RT}{4F} \right) \ln \left(\frac{p_1}{p_0} \right) - \left(\frac{RT}{4F} \right) \ln \left[1 + \left(\frac{RTA_2}{4FV\omega p_0} \right) \cos \omega t \right] \tag{46}$$

where p_0 is the mean internal (reference) pressure. For small amplitude (≤ 2.3 mV at 800 °C) of the EMF variation, equation (46) simplifies to

$$E = \left(\frac{RT}{4F} \right) \ln \left(\frac{p_1}{p_0} \right) - \left(\frac{RT}{4F} \right)^2 \left(\frac{A_2}{V\omega p_0} \right) \cos \omega t. \tag{47}$$

Equation (47) consists of two terms. The first

$$E_0 = (RT/4F) \ln(p_1/p_0) \tag{48}$$

is the mean value of the observed EMF. The second

$$B \cos \omega t = (RT/4F)^2 (A_2/V\omega p_0) \cos \omega t \quad (49)$$

is the sinusoidal variation of the EMF about the mean. Thus equation (47) may be written

$$E = E_0 - B \cos \omega t. \quad (50)$$

The two terms may be separated by appropriate signal processing, the amplitude B allowing determination of p_0 while E_0 reveals p_1/p_0 and hence p_1 . A simulation of the behaviour is shown in figure 15.

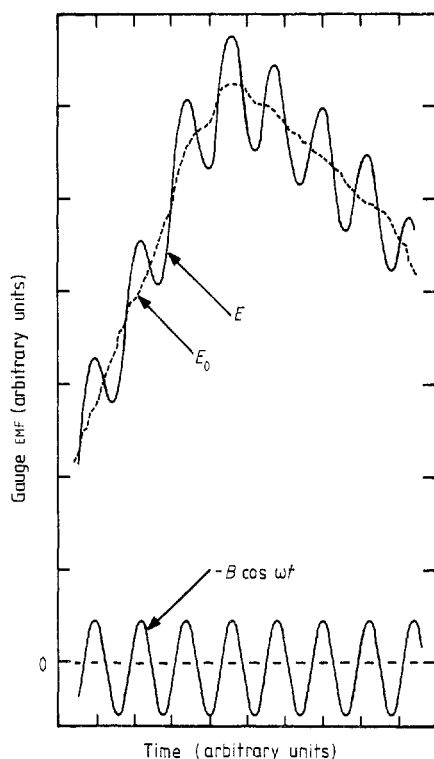


Figure 15. Simulation of the gauge output of a pump-gauge device with a sinusoidal current applied to the pump.

6. Impedance-based devices

Badwal and De Bruin (1979) have described a device consisting simply of an oxygen-ion conducting wafer coated on each side with a thin layer of Pd. This is operated at a temperature sufficiently elevated to promote substantial ionic conductivity in the ceramic. They found (see also De Bruin and Badwal 1980) that the electrode impedance increased by approximately two orders of magnitude when the Pd was oxidised to PdO, the behaviour being reversible. Measurements were readily made by applying an AC signal at low frequencies (5–100 Hz) as shown in figure 16.

The point at which the transition between Pd and PdO occurs is strictly defined by the thermodynamics of the reaction, the temperature depending upon the oxygen partial pressure. This technique for the determination of p_{O_2} is absolute and requires no reference gas.

A further refinement involves the addition of a third pseudo-reference electrode (Badwal and De Bruin 1982). This allows the working electrode to be biased permitting alteration of the oxidation–reduction point with consequent improved versatility.

The response time of these devices is likely to be slow because the oxidation–reduction effectively has a high pseudo-capacitance. However, in some applications this is not a critical factor.

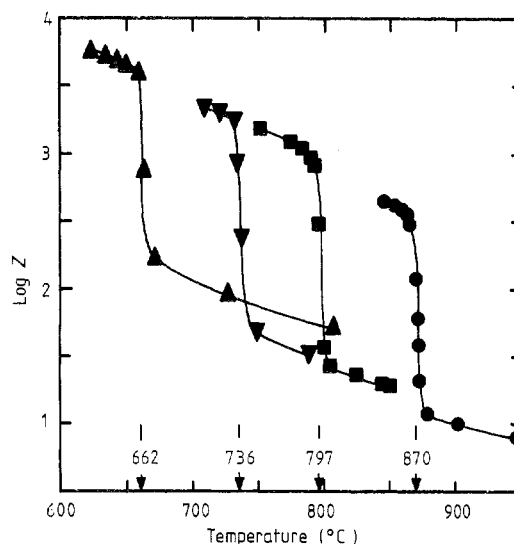
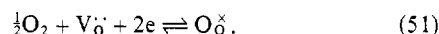


Figure 16. Impedance–temperature behaviour at 10 Hz for a Pd/zirconia/Pd cell. Sample gas pressure (atm) (10^5 Pa = 1 atm): ●, 1; ■, 0.208; ▼, 0.049; ▲, 0.0046. (Diagram courtesy Academic Press, Inc.)

Another impedance-based sensor has recently been discussed by Goge *et al* (1985). It consists of a cermet composed of Pt and zirconia. This is exposed to the sample gas and the DC resistance measured. The current traverses the cermet via oxygen ions in the ceramic and electrons in the metal. Consequently there is an interfacial impedance at each contact between the two solid phases due to the reaction (Maskell *et al* 1987a)



Electrode impedance has been shown to vary as $p_{O_2}^{-1/2}$ (Verkerk *et al* 1983, Kaneko *et al* 1986) and consequently with calibration allows determination of p_{O_2} .

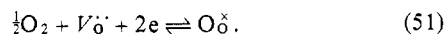
The simplicity of this device is an attractive feature. A possible problem is that electrode impedance is normally sensitive to contaminants and the system may be poisoned by components resulting from the oxidation of fossil fuels.

Appendix

The factors influencing the response of a potentiometric sensor are discussed below. It is not possible to quantify, in general terms, the relative magnitudes of each: these depend on the specific operating conditions pertaining such as temperature, gas concentration range, sampling or non-sampling system, etc. However, the list provides a basis for the systematic identification of the controlling processes in future studies.

A1. Double layer capacitance

The following discussion is based upon considerations of Steele *et al* (1981). At the interface between an electronic conductor and an electrolyte there is, in general, a separation of charge in the latter balanced by an equal and opposite charge in the electronic conductor. This double layer behaves as a capacitor and can store charge. When a change in p_1 occurs at the electrode–electrolyte boundary the potential of the electrode changes and charge moves in or out of the double layer with a corresponding current on the electrode. This current is dissipated in an electrochemical reaction

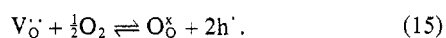


Electrons are supplied from the electronic conductor. There is an electrical resistance to this reaction, related to the

overpotential and the current, so that the system behaves as a parallel $R-C$ combination and consequently displays an RC time constant. In fact RC is the time taken for transport of $(1-1/e)$ or 63% of the charge between the two equilibrium states (see standard texts on electricity, e.g. Fewkes and Yarwood 1956).

A2. Stoichiometry changes in the double layer

The equilibrium between the oxygen-ion conductor and the gas phase can be expressed as



The equilibrium constant, K , for this process is

$$K = [O\ddot{O}] [h']^2 / [V\ddot{O}] p_{O_2}^{1/2} \quad (52)$$

Thus, the stoichiometry of the oxide varies with p_{O_2} , the extent depending upon the value of K which varies from one oxide to another: with ZrO_2 -based or Bi_2O_3 -based materials changes in stoichiometry will be small in the first case but substantial in the second.

Clearly, when a change in p_{O_2} is made then given sufficient time an equilibrium is established throughout the ionic conductor. However, as has been noted, if $t \approx 1$ then as far as the EMF is concerned only changes in the double layer region are important; this region must come to chemical equilibrium with the gas phase before a stable EMF can be established and this may effectively introduce a further capacitance with a consequent delay in the response.

A3. Effect on the gas phase of changes in stoichiometry

At short times after a change in p_{O_2} the $[h']$ profile at the interface is very steep. These holes are minority carriers and hence move by diffusion (Heyne and Beekmans 1971). There are two consequences of the high diffusion rate of holes at the interface. The first is that a significant electrode overvoltage results due to charge transfer, which perturbs the measured EMF. The second is that a p_{O_2} gradient is set up in the gas phase adjacent to the electrode-electrolyte interface, which results in a diffusion overvoltage. Both the above overvoltages effectively slow the electrode response.

A4. Electrode reversibility

The electrode reaction involves several consecutive steps (Pizzini 1973, Gur *et al* 1980) any of which may, in principle, be rate determining. In practice the particular rate-determining step depends upon the parameters of the system. A low electrode resistance is necessary to reduce the RC time constant and allow rapid electrode response. In order to achieve this, in practical sensors care must be taken to ensure a long three-phase boundary (i.e. electrolyte-electrode-gas) and this entails the preparation of a thin porous electrode. Response time deteriorates if the electrode contains glassy material, sometimes added to aid adhesion, as this blocks three-phase sites. Also, if pretreated at too high a temperature the composite particles of the electrode (e.g. Pt) may sinter resulting in reduced porosity.

A5. Hydrodynamics in the gas phase

Before the electrode can respond to a p_{O_2} change, that change must be transmitted to the electrode surface. In many practical situations (e.g. $p_{O_2} \geq 10^2$ Pa, $ZrO_2-Y_2O_3$ ceramic, 700 °C) it is the hydrodynamics in the gas phase that limits the sensor response. For example, in a sampling system the gas must pass along a tube before it reaches the sensing electrode: the response is limited by the time taken for the gas to traverse the tube; less obviously the front carrying the p_{O_2} change becomes diffuse as a result of viscosity effects in the tube; finally the gas may not impinge directly onto the sensing electrode so as to avoid

cooling the electrode. Consequently there is also a diffusion step which delays the transmission of the p_{O_2} change to the electrode. On the other hand, at low p_{O_2} values (e.g. < 10 Pa in mixture with an inert gas) or at low temperatures (< 500 °C, ZrO_2 -based sensor) the electrode response may be limiting.

In practical sensors the electrodes are sometimes coated with a porous layer for protection. This additional coating acts as a diffusion barrier and also delays response. However, the diffusion coefficient of oxygen at ~ 700 °C is very high (~ 100 mm² s⁻¹) and response delays due to a porous barrier are usually short.

References

- Anderson J E and Graves Y B 1981
J. Electrochem. Soc. **128** 294
- Anderson J E and Graves Y B 1982
J. Appl. Electrochem. **12** 335
- Badwal S P S, Bannister M J and Garrett W G 1984
Science and Technology of Zirconia II, Advances in Ceramics, vol. 12 ed. N Claussen *et al* (Columbus, Ohio: Am. Ceram. Soc.) p 598
- Badwal S P S and De Bruin H J 1979
Aust. Chem. Eng. **20** 9
- Badwal S P S and De Bruin H J 1982
J. Electrochem. Soc. **129** 1921
- Bauerle J E 1969
J. Phys. Chem. Solids **30** 2657
- Crank J 1956 *The Mathematics of Diffusion* (Oxford: Oxford University Press) p 48
- De Bruin H J and Badwal S P S 1980
J. Solid State Chem. **34** 133
- De Jong H L 1983 US Patent Specification 4 384 935
- Dietz H 1982
Solid State Ionics **6** 175
- Dietz H, Haecker W and Jahnke H 1977 *Advances in Electrochemistry and Electrochemical Engineering*, vol. 10 ed. H Gerischer and C W Tobias (New York: Wiley) pp 1-90
- Fewkes J H and Yarwood J 1956 *Electricity and Magnetism* vol. 1 (London: University Tutorial) p 123ff
- Fleming W J 1977
J. Electrochem. Soc. **124** 21
- Fouletier J 1982/3
Sensors and Actuators **3** 295
- Fouletier J, Fabry P and Kleitz M 1976
J. Electrochem. Soc. **123** 204
- Fouletier J, Seinerer H and Kleitz M 1974
J. Appl. Electrochem. **4** 305
- Goge M, Especel D, Heggstadt K and Gouet M 1985
Transport-Structure Relations in Fast Ion and Mixed Conductors ed. F W Poulsen *et al* (6th Risø Int. Symp. On Met. and Mat. Sci., Risø Nat. Lab.) p 291
- Gur T M, Raistrick I D and Huggins R A 1980
J. Electrochem. Soc. **127** 2620
- Haaland D M 1977
Anal. Chem. **49** 1813
- Haaland D M 1980
J. Electrochem. Soc. **127** 796
- Hetrick R E, Fate W A and Vassell W C 1981
Appl. Phys. Lett. **38** 390
- Hetrick R E, Fate W A and Vassell W C 1982
IEEE Trans. Electron Devices **ED-29** 129

Heyne L 1976 *Measurement of Oxygen* ed. H Degn *et al* (*Proc. Int. Symp., Odense Univ. 1974*) (Amsterdam: Elsevier) p 65

Heyne L 1978
Paper presented at the Electrochem. Soc., Spring Meeting, Seattle Abs. No 78

Heyne L and Beekmans N M 1971
Proc. Brit. Ceram. Soc. **19** 229

Heyne L and den Engelsen D 1977
J. Electrochem. Soc. **124** 727

Issacs H S and Olmer L J 1982
J. Electrochem. Soc. **129** 436

Kaneko H, Maskell W C and Steele B C H 1987
Solid State Ionics **22** 161

Kleitz M, Bernhard H, Fernandez E and Schouler E 1981
Science and Technology of Zirconia, Advances in Ceramics vol. 3 ed. A Heuer and L W Hobbs (Columbus, Ohio: Amer. Ceram. Soc.) p 310

Kubaschewski O and Alcock C B 1979 *Metallurgical Thermochemistry* 5th edn (Oxford: Pergamon)

Kumata S, Miura N, Yamazoe N and Seiyama T 1984
Chem. Lett. 981

Maskell W C, Kaneko H and Steele B C H 1986
Proc. 2nd Int. Meeting on Chemical Sensors ed. J L Aucouturier *et al* (Bordeaux Chemical Sensors, University of Bordeaux) p 302

Maskell W C, Kaneko H and Steele B C H 1987b
J. Appl. Electrochem. **17** 489

Maskell W C, Sammes N M and Steele B C H 1987a
J. Phys. D: Appl. Phys. **20** 99

Maskell W C and Steele B C H 1986
J. Appl. Electrochem. **16** 475

Mogab C J 1973
J. Vac. Sci Technol. **10** 852

Moore W J 1972 *Physical Chemistry* 5th edn (London: Longman) pp 99ff and 528ff

Pizzini S 1973 *Fast Ion Transport in Solids* ed. W van Gool (Amsterdam: North Holland) p 461ff

Ramanarayanan T A, Narula M L and Worrell W L 1979
J. Electrochem. Soc. **126** 1360

Saji K, Kondo H, Takahashi H, Takeuchi T and Igarashi I 1985
Proc. Int. Conf. Solid-State Sensors and Actuators, Philadelphia, 11–14 June 1985 (New York: IEEE) p 336

Sandler Y L 1971
J. Electrochem. Soc. **118** 1378

Siebert E and Fouletier J 1983
Solid State Ionics **9/10** 1291

Soejima S and Mase S 1985
SAE Paper 850378

Steele B C H, Drennan J, Slotwinski R K, Bonanos N and Butler E P 1981 *Science and Technology of Zirconia, Advances in Ceramics* vol. 3 ed. A Heuer and L W Hobbs (Columbus, Ohio: Amer. Ceram. Soc.) p 286

Takeuchi T, Saji K, Igarashi I and Uchida K 1978 *Extended Abs. Electrochem. Soc., Fall Meeting, Pittsburgh* (Princeton, NJ: Electrochemical Society) **78–2** Abs. No 74

Verkerk M J and Burggraaf A J 1983
J. Electrochem. Soc. **130** 78

Verkerk M J, Hammink M W J and Burggraaf A J 1983
J. Electrochem. Soc. **130** 70

Wang D Y and Nowick A S 1979
J. Electrochem. Soc. **126** 1166

Williams D E and McGeehin P 1984 *Electrochemistry* (London: Royal Society of Chemistry) pp 246–90

Winnubst A J A, Scharenborg A H A and Burggraaf A J 1985
J. Appl. Electrochem. **15** 139



at Imperial College, London and is now Reader in Energy Technology at Middlesex Polytechnic.

William Maskell took a BSc in Physics at King's College, London. He joined the Ever Ready Company in 1969 working on research and development projects relating to batteries: while there he obtained a PhD in Chemistry as an external student of London University. He was awarded a Wolfson Research Fellowship in 1983 to develop solid state electrochemical oxygen sensors